

RESEARCH

Open Access

Robust motion estimation on a low-power multi-core DSP

Francisco D Igual*, Guillermo Botella, Carlos García, Manuel Prieto and Francisco Tirado

Abstract

This paper addresses the efficient implementation of a robust gradient-based optical flow model in a low-power platform based on a multi-core digital signal processor (DSP). The aim of this work was to carry out a feasibility study on the use of these devices in autonomous systems such as robot navigation, biomedical assistance, or tracking, with not only power restrictions but also real-time requirements. We consider the C6678 DSP from Texas Instruments (Dallas, TX, USA) as the target platform of our implementation. The interest of this research is particularly relevant in optical flow scope because this system can be considered as an alternative solution for mid-range video resolutions when a combination of in-processor parallelism with optimizations such as efficient memory-hierarchy exploitation and multi-processor parallelization are applied.

Keywords: Motion estimation, Digital signal processors, Bio-inspired systems

1 Introduction

Motion estimation has been deeply investigated during the last 50 years; however, it is still considered by the scientific community as an emerging field of special interest due to the plethora of applications that supports the interpretation of the real world, such as navigation, sports tracking, surveillance, video compression, robotics, vehicular technology, etc. It is also useful in the neuroscience field, where the task of modeling neuromorphic algorithms and systems, which fit well according to the human brain evidences, is an open and common research problem.

Motion estimation determines motion vectors and describes the transformation of an entire two-dimensional (2D) image into another, usually taken from contiguous frames in a video sequence using pixels or specific parts such as shaped patches or rectangular blocks.

Motion relies on three dimensions, but images are a projection of the three-dimensional scene onto a two-dimensional plane, therefore posing a mathematically ill-posed problem [1-3], usually known as 'aperture problem'. To overcome these drawbacks, external knowledge regarding the behavior of objects, such as rigid body constraints or other models that might approximate the

motion of a real video camera, becomes necessary. These models are based on the motion of rotation, translation, and zoom, in all three dimensions.

The *optical flow* paradigm is not exactly the same concept as motion estimation, although they frequently come up associated. Optical flow is the apparent motion of image objects or pixels between frames [3]. Two assumptions are usually applied to optical flow [4]:

- *Brightness constancy*: although the 2D position of the image discriminant characteristics, such as brightness, color, etc., may change, they keep their value constant over time. Algorithms for estimating optical flow exploit this assumption in various ways to compute a velocity field that describes the horizontal and vertical motions of every pixel in the image.
- *Spatial smoothness*: it appears from the observation that pixels in the neighborhood usually belong to the same surface and are inclined to present the same image motion.

Optical flow has many drawbacks that increase the burden of estimating it. For instance, the optical flow is ambiguous in homogeneous image regions due to the brightness constancy assumption. Additionally, in real scenes, the assumption is violated at the motion boundaries as well as by occlusions, noise, illumination changing, reflections, shadows, etc. Therefore, only

*Correspondence: figual@ucm.es

Depto. Arquitectura de Computadores y Automática,
Universidad Complutense de Madrid, Madrid 28040, Spain

the synthetic-made motion can be recovered with no ambiguity. These two assumptions may lead to errors in the flow estimates.

There are a number of common examples which deliver a non-null value for motion estimation but a zero value for optical flow, e.g., a rotating sphere under constant illumination. Similarly, a static sphere with changing light will deliver optical flow, while the motion field remains null [1], or an old barber pole in motion that shows a real velocity field perpendicular to the estimated optical flow.

Classifying the state of the art in algorithms and techniques, we find a common taxonomy used to estimate optical flow. They generally fall into one of the following categories:

- *Pattern-matching methods* [3] are probably the most intuitive methods. They operate by comparing the positions of image structure between adjacent frames and inferring velocity from the change in location. The aim of block-matching methods is to estimate motion vectors for each macro-block within a specific and fixed search window in the reference frame. These exhaustive or semi-exhaustive search algorithms match all macro-blocks within a search window in the reference frame to estimate the optimal macro-block in order to fit with the minimum block-matching error metric.
- *Motion energy methods* are probabilistic methods that use space-time oriented filters tuned to respond optimally to specific image velocities. Banks of such filters are used to respond to a range of visual motion possibilities [1]. Therefore, motion estimation is not unique for every single stimulus. These methods usually work under Fourier space.
- *Gradient-based or differential technique* family uses derivatives of image intensity in space and time. Combinations and ratios of these derivatives yield explicit measures of velocity [2,5]. The particular implementation of the algorithm used in this paper belongs to this family and is based on Johnston's work [6,7]. The *multi-channel gradient model* (McGM) was developed as part of a research effort aimed at improving our understanding of the human visual system. This model also allows us to make predictions that can be tested through psychophysical experimentation as separate motion illusions that are observed by humans in experiments [8].

One of the main drawbacks of the McGM model is the high hardware requirements needed to achieve real-time processing. On one hand, McGM presents an uptrend in temporal data storage which is translated into non-negligible memory requirements; on the other hand, optical flow processing requires important computational

capabilities to meet real-time requirements. Previous works [9,10] have fulfilled those requirements by means of exploitation of inherent data parallelism of McGM using both modern multi-core processors and hardware accelerators such as field-programmable gate arrays (FPGAs) and graphics processing units (GPUs).

The limitation in power consumption of current embedded devices makes it necessary to consider energy-related issues in the implementation of optical flow algorithms. There are in the literature *ad hoc* solutions to solve the motion estimation problem with power constraints. As an example, there are countless proposals under low-power conditions for pattern-matching family algorithms, but most are in the video compression field [11,12]. Another approach with central processing units (CPUs) [13] presents a parallel scheme applied to a model based on well-known Lucas-Kanade approach, which reduces power consumption in terms of thermal design power (TDP) and still meets the real-time requirements when low-power chipsets (TDPs of 20 to 30 W) are used. Moreover, Honegger et al. [14] implement a low-power stereo vision system with FPGA based on the Nios II processor (Altera, San Jose, CA, USA). Furthermore, processor manufacturers are now concerned for concepts such as *green computing*. The aim is to develop more efficient chips not only in terms of performance rates (throughput measured in terms of floating-point operations per second (FLOPS) or Mbits per second) but also energy efficiency [15]. Besides modern and efficient multi-core CPUs, hardware accelerators such as GPUs or Intel MIC (Intel Corp., Santa Clara, CA, USA), or reconfigurable devices (FPGAs), one of the latest additions on specific-purpose architectures applied to general-purpose computing are low-power digital signal processors (DSPs). One of the primary examples in this field is the C6678 multi-core DSP from Texas Instruments (TI; Dallas, TX, USA) that combines a theoretical peak performance of 128 GFLOPs (billions of floating-point operations per second) with a power consumption of roughly 10 W per chip. Besides, one of the most appealing features is the ease of programming, adopting well-known programming models for sequential and parallel implementations.

Our contribution provides an efficient implementation for an optical flow gradient-based model using a low-power DSP exploiting different levels of parallelism. To the best knowledge of the authors, this is the first attempt to use a DSP architecture to implement a robust optical flow gradient-based model. There are only few approaches existing in the literature exploiting gradient-based motion estimation methods in DSP platforms as the one proposed by Shirai et al. [16] in early 1990s, implementing the classical method of Horn-Schunck algorithm [17] using many boards with a TMS320C40 DSP each. This algorithm supplements optical flow constraint with regularizing smooth

terms, while our work uses spatio-temporal constancy. Besides, performance and/or energy consumption is not considered in that work. Rowenkap et al. [18] implemented in 1997 the same algorithm as the previous work, using the same DSP and reaching up a throughput of 5 frames per second (fps) and 15 fps (for 128^2 image resolution) when using one and three DSPs, respectively. The last work considered is the neuromorphic implementation of Steiner [19] that uses the Srinivasan algorithm [20] on a dsPIC33FJ128MC804 processor; this algorithm is based on simple stage procedure of image interpolation.

The challenge addressed in this paper is based on the efficient exploitation of available resources in TI's C6678 DSP, taking into account the particular features of McGM:

- Exploit loop-level parallelism by means of a very long instruction word (VLIW) processor capability available in TI's C6678 DSP.
- Take advantage of data-level parallelism by means of multi-media extensions capability.
- Make use of thread-level parallelism available in TI's C6678 multi-core DSP.
- Exploit the memory system hierarchy with the efficient use of cache levels and on-chip shared memory.

Our experimental evaluation includes a comparison of the DSP implementation with other state-of-the-art architectures, including general-purpose multi-core CPUs and other low-power architectures.

The rest of the paper is organized as follows. Section 2 moves through a specific neuromorphic model and describes the particularities of each stage. Section 3 gives an overview of the DSP architecture, together with the main motivations for choosing this platform for our motion estimation approach. In Section 4, we give details about the specifics of the implementation of McGM on the DSP and provide an experimental analysis of the implementation. Finally, Section 5 provides some concluding remarks and outlines future research lines.

2 Multi-channel gradient model

The McGM model, proposed by Johnston et al. [6,7], implements a processing vision scheme described by Hess and Snowden [21], combining the interaction between ocular vision and brain perception and simplifying the human vision model [8]. In order to solve the problems with the basic motion constraint equation, many gradient measurements have been introduced (Gaussian derivatives) into the velocity measure via Taylor expansion representation of the local space-time structure.

Figure 1 shows a simplified scheme of the necessary stages to be completed. From the point of view of data

processing, the McGM algorithm involves an increasing temporal data generation in each stage. Hence, this algorithm may be considered as a data-expansive processing algorithm. Moreover, the nature of its dataflow makes it essential to fully conclude a given stage before starting the next one, which inhibits the ability to apply latency reduction techniques similar to those addressed in a pipelined processor since the stage time differs substantially. The only way to reduce motion estimation latency is to minimize the computation time at stage level. This work focuses on optimal exploitation of the high data- and loop-level parallelism available in each McGM stage. In order to clarify these aspects, Figure 2 shows the processing dataflow, while the memory consumption at each stage is detailed in next subsections.

2.1 FIR-filtering temporal

In the *finite impulse response (FIR)-filtering temporal* stage, the McGM algorithm models three different temporal channels based on the experiments carried out by Hess and Snowden [21] about visual channels discovered in human beings: one *low-pass filter* and two *band-pass filters* with a center frequency of 10 and 18 Hz, respectively. Input signal is filtered according to Equation 1, where α and τ represent the peak and spread of the log-time Gaussian function, respectively.

$$k(t) = \frac{e^{-\left(\frac{\log(t/\alpha)}{\tau}\right)^2}}{\sqrt{\pi}\alpha e^{\left(\frac{\tau^2}{4}\right)}} \quad (1)$$

In practice, for an input movie of N frames with $n_x \times n_y$ resolution, this stage produces approximately $(N - L) \times n_x \times n_y \times n_{\text{Temp_filt}}$ temporal data as indicated in Figure 2 as $T1$, $T2$, and $T3$ ($n_{\text{Temp_filt}} = 3$) in *temporal filtering stage*; these intermediate data structures are provided to the *spatial filtering* stage as inputs.

2.2 FIR-spatial derivatives

The *FIR-spatial derivative* stage is based on space domain computation where the shape of the receptive fields from the primitive visual cortex is modeled using either Gabor functions or a derivative set of Gaussians [22]. A kernel function

$$\text{kernel} = \frac{e^{-\left(\frac{x^2+y^2}{2\sigma^2}\right)}}{\sigma\sqrt{2\pi}} \quad (2)$$

is derived to obtain upper order differential operators using Hermite polynomials. In our case, the n th derivative

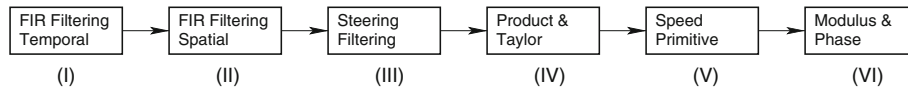


Figure 1 Scheme of the multi-channel gradient model with several stages.

can be obtained by multiplying the corresponding Hermite polynomial by the original Gaussian function:

$$\begin{aligned} \frac{d^n}{dx^n}(G_0) &= \frac{d^n}{dx^n} \left(\frac{e^{-\left(\frac{x^2+y^2}{2\sigma^2}\right)}}{\sigma\sqrt{2\pi}} \right) \\ &= H_n \left(\frac{x}{\sqrt{2}\sigma} \right) H_n \left(\frac{y}{\sqrt{2}\sigma} \right) \left(\frac{-1}{\sqrt{2}\sigma} \right)^{2n} \left(\frac{e^{-\left(\frac{x^2+y^2}{2\sigma^2}\right)}}{\sigma\sqrt{2\pi}} \right) \end{aligned} \quad (3)$$

being σ the variance in normal distribution.

From the point of view of data-path processing, for $n\text{Spat_filters}$ Gaussian filters (see Figure 2), this stage generates $(N - L) \times nx \times ny \times n\text{Temp_filters} \times n\text{Spat_filters}$ output data.

2.3 Steering filtering

The *steering filtering* stage synthesizes filters at arbitrary orientations formed by a linear combination of other filters in a small *basis* set. More specifically, if we call m and n the order in directions x and y , respectively, θ the projected angle and D the derivative operator, the general expression is obtained as a linear combination of one filter on the same order basis (G_0), see Equation 4.

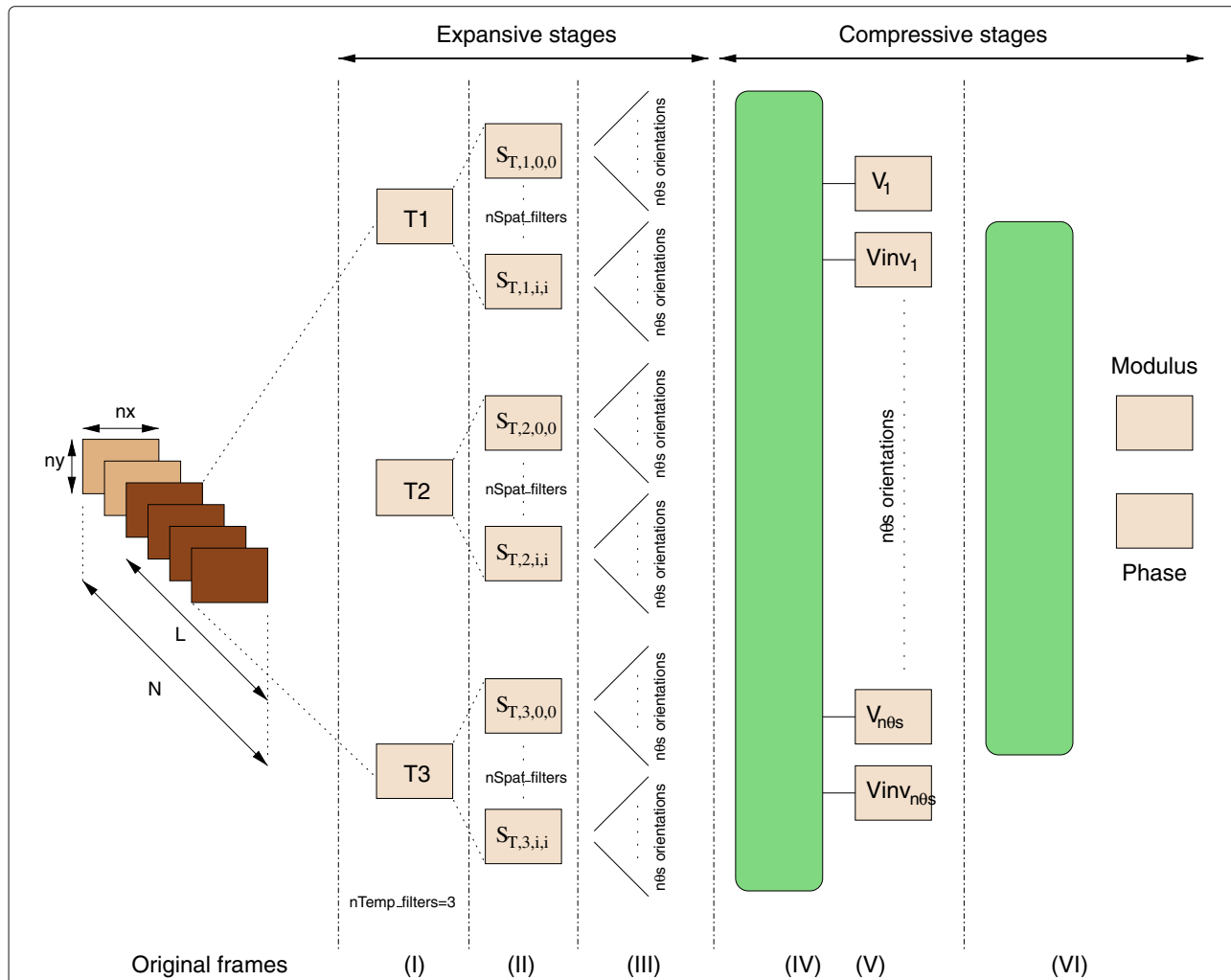


Figure 2 Data processing in the multi-channel gradient model through several stages. (I) Temporal filtering, (II) spatial filtering, (III) steering, (IV) product and Taylor, (V) speed and inverse speed, and (VI) velocity and direction.

$$G_{n,m}^{\theta} = \left[\sum_{k=0}^n \binom{n}{k} (D_x \cos \theta)^k (D_y \sin \theta)^{n-k} \right] * \left[\sum_{i=0}^m \binom{m}{i} (-D_x \sin \theta)^i (D_y \cos \theta)^{m-i} \right] G_0 \quad (4)$$

From the data-path perspective, this is the most memory-consuming and computational-demanding stage. Resource consumption is closely related to the number of orientations to consider, which is denoted by $n\theta$ s orientations in Figure 2. More specifically, the amount of data produced at this stage is quantified close to $((N-L) \times nx \times ny \times nTemp_filters \times nSpat_filters \times n\theta s)$.

2.4 Product and Taylor and quotients

$$I(x+p, y+q, t+r) = \sum_{i=0}^l \sum_{j=0}^m \sum_{k=0}^n \frac{p^i q^j r^k}{i! j! k!} \frac{\partial^n}{\partial x^i \partial y^j \partial t^k} I(x, y, t) \quad (5)$$

Quotient calculation is the last stage derived from the common pathway. The goal here is to compute a quotient for every sextet's component:

$$\begin{matrix} X = \partial I / \partial x \\ Y = \partial I / \partial y \\ T = \partial I / \partial t \end{matrix} \rightarrow \begin{matrix} XX & XY & XT \\ YY & YT & TT \end{matrix} \rightarrow \begin{matrix} YT/TT & XY/XX & XT/XX \\ YT/YY & XY/YY & XT/TT \end{matrix} \quad (6)$$

From the point of view of dataflow, McGM changes its trend at this point and starts to converge, which means a considerable reduction in the amount of data to compute. Data stored is approximately $(N-L) \times nx \times ny \times n\theta s \times 6$.

2.5 Velocity primitives

The *velocity primitive* stage implements the modulus and phase estimation with separate expressions. After that, speed measurements - parallel and orthogonal to the primary directions - are taken to yield a vector of speed measures (parallel and orthogonal speed components.)

$$\hat{s} = (\hat{s}_{\parallel}, \hat{s}_{\perp}) \quad (7)$$

The raw measurements of speed are also conditioned by including the measurements of the image structure XY/XX and XY/YY where the final conditioned speed vectors results in the number of orientations at which the speed is evaluated:

$$\begin{aligned} \hat{s}_{\parallel} &= \sqrt{\frac{2}{\Sigma}} \left[\frac{XT}{XX} \left(1 + \left(\frac{XY}{XX} \right)^2 \right)^{-1} \right] \\ \hat{s}_{\perp} &= \sqrt{\frac{2}{\Sigma}} \left[\frac{YT}{YY} \left(1 + \left(\frac{XY}{YY} \right)^2 \right)^{-1} \right] \end{aligned} \quad (8)$$

Inverse speed is calculated in a similar way:

$$\check{s}_{\parallel} = \sqrt{\frac{2}{\Sigma}} \left[\frac{XT}{TT} \right] \quad \check{s}_{\perp} = \sqrt{\frac{2}{\Sigma}} \left[\frac{YT}{TT} \right] \quad (9)$$

Modulus and phase extraction corresponds to the final velocity vector, which is computed from the velocity components previously calculated.

Velocity primitives are allocated with $(N-L) \times nx \times ny \times n\theta s \times 4$ data.

2.6 Modulus and phase

Finally, the motion modulus is calculated through a quotient of determinants:

$$Modulus^2 = \frac{\begin{vmatrix} \hat{s}_{\parallel} \cos \theta & \hat{s}_{\parallel} \sin \theta \\ \hat{s}_{\perp} \cos \theta & \hat{s}_{\perp} \sin \theta \end{vmatrix}}{\begin{vmatrix} \hat{s}_{\parallel} \check{s}_{\parallel} & \hat{s}_{\parallel} \check{s}_{\perp} \\ \hat{s}_{\perp} \check{s}_{\parallel} & \hat{s}_{\perp} \check{s}_{\perp} \end{vmatrix}} \quad (10)$$

The direction of motion is extracted by calculating a measurement for phase that is then combined across all speed-related measures:

$$phase = \arctan \left(\frac{(\check{s}_{\parallel} + \hat{s}_{\parallel}) \sin \theta + (\check{s}_{\perp} + \hat{s}_{\perp}) \cos \theta}{(\check{s}_{\parallel} + \hat{s}_{\parallel}) \cos \theta - (\check{s}_{\perp} + \hat{s}_{\perp}) \sin \theta} \right) \quad (11)$$

Lastly, modulus and phase are size of $(N-L) \times nx \times ny$ (one piece of data per input pixel).

3 Overview of the C6678 DSP architecture

The C6678 digital signal processor from Texas Instruments is a high-performance, low-power DSP with floating-point capabilities [23]. It presents eight C66x VLIW cores and runs at 1 Ghz. The whole device dissipates a maximum power of 10 W. Besides low-power, high-performance, and floating-point capabilities, one of the strengths of the C6678 device is the amount of standard peripherals it supports: PCIe interface to communicate with a CPU host, Serial Rapid I/O, and Hyperlink for fast- and low-latency inter- and intra-chip communication, or direct memory access (DMA) to overlap

computation with transfers between the external memory and on-chip memory.

3.1 C66x core architecture

The C66x core illustrated in Figure 3 is the base of the multi-core C6678 DSP architecture. It is implemented as a VLIW architecture, taking advantage of different levels of parallelism:

- *Instruction-level parallelism.* In the core, eight different functional units are arranged in two independent sides. Each one of the sides has four processing units, namely L, M, S, and D. The M units are devoted to multiplication operations. The D unit performs address calculations and load/store instructions. The L and S units are reserved for additions and subtractions, logical, branch, and bitwise operations. Thus, this eight-way VLIW machine can issue eight instructions in parallel per cycle.
- *Data-level parallelism.* The C66x instruction set (ISA) includes single-instruction multiple-data (SIMD) instructions that operate on 128-bit vector registers. More precisely, the M unit, performs four single-precision (SP) multiplications (or one double precision (DP) multiplication) per cycle. L and S units

carry out two SP additions (or one DP addition) per cycle. Thus, the C66x is ideally able to perform eight single-precision multiply-add (MADD) operations in 1 cycle. In double precision, this number is reduced to two MADDs in 1 cycle. With eight C66x cores, a C6678 processor running at 1 GHz yields 128 SP GFLOPS or 32 DP GFLOPS. All floating-point operations support the IEEE754 standard.

- *Thread-level parallelism.* It can be exploited by running different threads across the cores of the DSP. In our case, we will use OpenMP as the tool to manage thread-level parallelism.

3.2 Memory hierarchy

The memory hierarchy for the C6678 device is shown in Figure 3 (left). L1 cache is divided into 32 KB of L1 program cache and 32 KB of L1 data cache per core. There is also 512 KB of L2 cache per core. Both L1 data cache and L2 memory can be configured either as random-access memory (RAM), cache, or part RAM/part cache. This provides additional capability of handling memory and can be exploited by the programmer. There is an on-chip shared memory of 4,096 KB accessible by all cores, known as multi-core shared memory controller (MSMC) memory, and an external 64-bit DDR3 memory interface running at 1,600 MHz with ECC support.

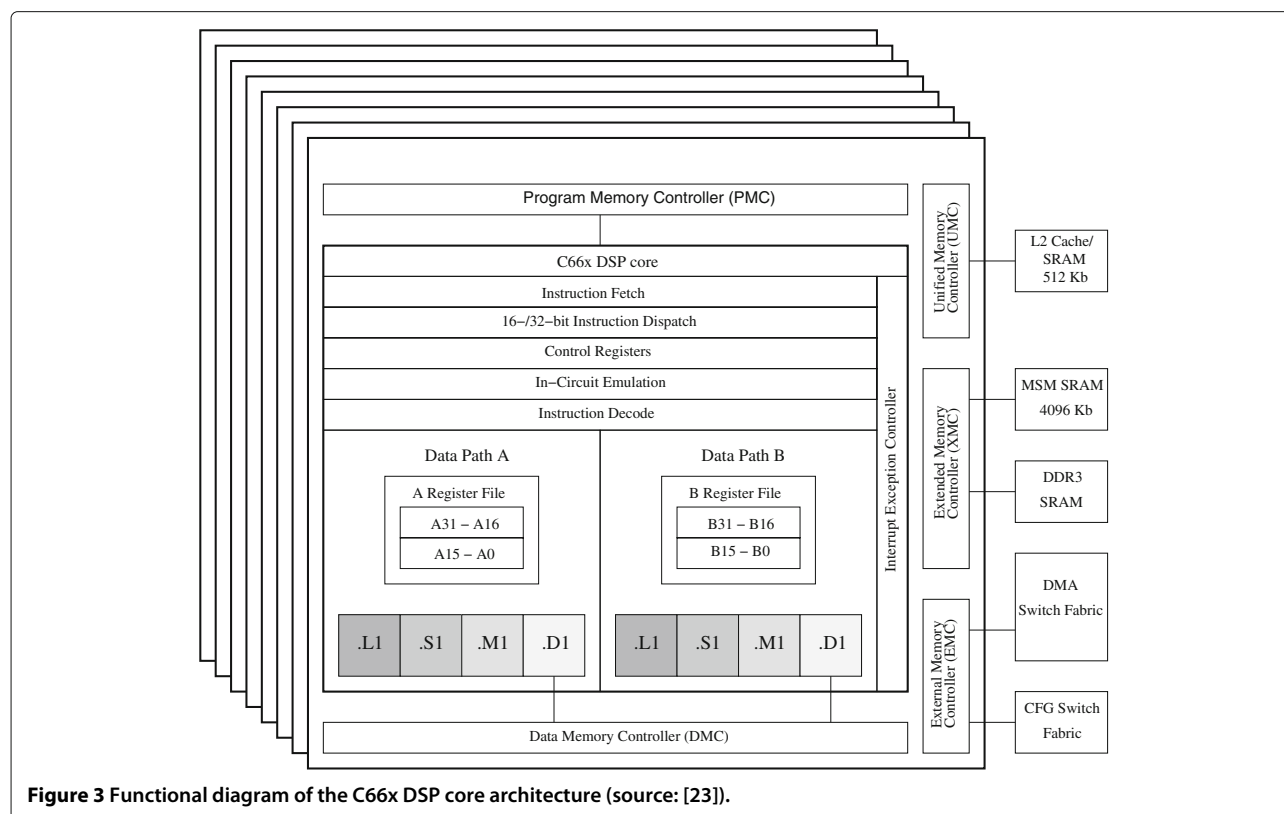


Figure 3 Functional diagram of the C66x DSP core architecture (source: [23]).

3.3 Programming the DSP

TI's DSPs run a lightweight real-time native operating system called SYS/BIOS. A C/C++ compiler is provided as part of the development environment. The C/C++ compiler eases the porting effort of virtually every existing C/C++ code to the architecture. To improve the efficiency of the generated code for each TI architecture, the compiler provides optimization techniques in the form of `#pragmas` and intrinsic SIMD instructions to fully exploit the core architecture and extract all the potential performance without resorting to assembly programming.

The compiler supports OpenMP 3.0 to allow rapid porting of existing multi-threaded codes to multi-core DSPs. The OpenMP runtime performs the appropriate cache control operations to maintain the consistency of the shared memory when required, but special precaution must be taken to keep data coherence for shared variables, as no hardware support for cache coherence across cores is provided.

3.4 Work environment

All codes were evaluated using a TMDXEVM6678LE evaluation module that includes an on-board C6678 processor running at 1 GHz. The board has 512 MB of DDR3 RAM memory available for image storage or generation. Our tests were developed on top of SYS/BIOS using the OpenMP implementation from Texas Instruments, MCSDK version 2.1, and Code Generation Tools version 7.4.1 with OpenMP support enabled. Single-precision floating-point arithmetic was used for all the experiments. We have not observed any precision issue in our DSP implementations compared with previous results in other architectures [9,24,25]. Therefore, our experimental section will be focused exclusively on a performance analysis instead of a qualitative analysis of the obtained numerical results.

4 Implementation and experimental results

In this section, we present relevant algorithmic and implementation details of each stage of the McGM method. Whenever possible, we provide a list of incremental optimizations applied in order to improve the performance of our implementation on the multi-core DSP. Due to the high-computational requirements of the first three stages of the algorithm (*temporal filtering*, *spatial filtering*, and *steering*), we will focus on those parts. However, some notes about the last stages, together with experimental results, are also given.

The optimizations proposed are DSP specific and address four of the most appealing features of the architecture: *instruction*, *data*, and *thread parallelism* extraction, and the exploitation of the flexibility of the *memory hierarchy*, plus the usage of DMA to overlap computation and communication.

4.1 Relevant parameters for McGM

Evaluating the performance of McGM is a hard task, mainly due to the large amount of parameters that can be modified in order to tune the algorithm behavior. Many of those parameters have a great impact not only on the precision of the solution but also on the overall attained performance. Table 1 lists the main configurable parameters associated with the first three stages of McGM. The column labeled as 'Typical values' provides an overview of the most common values, although different ones can be used to vary the motion estimation accuracy.

In Table 1, we also add four different parameter configurations that will be used for global throughput evaluation. Although all experimental results are reported for video sequences with square frames, our implementation is prepared for non-squared images, and no qualitative differences in the performance results have been observed.

Table 1 Main parameters involved in the McGM algorithm

Parameter	Description	Affects stage	Typical values	Selected configurations			
frames	Input frame set	All	-	Conf. 1	Conf. 2	Conf. 3	Conf. 4
N	Number of input frames	All	Depends on input		40		
$n_x \times n_y$	Frame dimensions	All	Depends on input		32^2 to 128^2		
L	Window (temporal convolution)	1	15 to 23	7	15	19	23
$n_{\text{Temp_filters}}$	Number of temporal filters	1-	3	3	3	3	3
T	Window (spatial convolution)	2	15 to 23	7	15	19	23
$n_{\text{Spat_filters}}$	Number of spatial filters	2-	6	6	6	6	6
$n_{\text{Ortho_Orders}}$	Number of orthogonal orders	3	3	3	3	3	3
$n\theta$ s	Number of angles	3-	6 to 24	6	12	18	24

4.2 McGM implementation on the DSP

The main implementation details and optimization techniques applied in our McGM porting task to the multi-core DSP are detailed in this section. As exposed in the algorithm description, we will divide the overall procedure into stages, describing each one in detail. Many of the optimization techniques applied for the DSP are quite similar for all stages. Therefore, the common optimization techniques are explained in detail next.

1. *Basic implementation.* We establish a baseline C implementation for comparison purposes. It includes the necessary compiler optimization flags and common optimization techniques to avoid unnecessary calculations and benefit from data locality and cache hierarchy. No further DSP-specific optimizations are applied in the code of this naive implementation.
2. *DMA and memory-hierarchy optimization.* One of the strengths of the DSP is the ability of explicitly managing on-chip memory levels (L1 cache, L2 cache, and MSMC memory). Thus, one can define buffers, assign them to a particular memory-hierarchy level (using the appropriate `#pragma` annotations in the code), and perform data copies between them as necessary. In addition, DMA capabilities are offered in order to overlap data transfers between memory levels and computation.
The usage of blocking and double-buffering is required. This involves the allocation of the current block of each frame to be processed and the next block which is being transferred through DMA while CPU computation is in progress. This technique effectively hides memory latencies, improving the overall throughput. In our case, we have mapped the temporal buffers that accommodate blocks of the input frames to the on-chip MSMC memory, in order to improve memory throughput in the computation stage.
3. *Loop optimization.* VLIW architectures require a careful loop optimization in order to let the compiler effectively apply techniques such as *software pipelining*, *loop unrolling*, and *data prefetching* [26]. In general, the aim is to keep the (eight) functional units of the core fully occupied as long as possible. To achieve this goal, the developer guides the compiler about safe loop unrolling factors, fixed unroll counts (using appropriate `#pragma` constructions), or pointer disambiguation (using `restrict` keyword on those pointers that will not overlap during the computation) by means of the mentioned tags or *pragmas*. Even though this type of optimizations is not critical in superscalar processors that defer the extraction of instruction-level

parallelism to execution time, it becomes crucial for VLIW architectures, even more for algorithms heavily based on loops as McGM. We have performed a full search to find the optimal unroll factor for each loop in the algorithm.

4. *SIMD vectorization.* As mentioned in Section 3, each C66x core is able to execute single-cycle arithmetic and load/store instructions on vector registers up to 128-bit wide. Naturally, this feature is supported at ISA level and can be programmed using intrinsics [26]. In McGM, data parallelism is massive and can be exploited by means of SIMD instructions in many scenarios. Intermediate data structures are stored using single-precision floating point (32-bit wide).
Thus, in the convolution step, input data can be grouped and processed in a SIMD fashion using 128-bit registers (usually referred as *quad* registers) for multiplications and 64-bit registers for additions. Given that the C66x architecture can execute up to eight SP multiplications (four per each M unit) and eight SP additions (two per each L and S unit), each core can potentially execute up to eight SP multiplication-additions per cycle if SIMD is correctly exploited. At this stage, we load and operate on four consecutive pixels of the image, unrolling the corresponding loop by a factor 4. Special caution must be taken in order to meet the memory alignment restrictions of the load/store vector instructions; to meet them, we apply zero-padding to the input image when necessary, according to its specific dimensions.
5. *Loop parallelization.* Up to this point, all the optimizations have been focused on exploiting parallelism at core level. The last stage of the optimization involves the exploitation of thread-level parallelism to leverage the multiple cores in the DSP. The parallelization is carried out by means of OpenMP. Special care must be taken with shared variables, as no cache coherence is automatically maintained. Thus, data structures must be zero-padded to fill a complete cache line and to avoid false sharing, and explicit cache write-back and/or invalidate operations must be performed in order to keep coherence between local memories to each core.

4.2.1 Stage 1: temporal filtering

Algorithm and implementation In order to obtain the temporal derivative of the image, it is necessary to perform a convolution of each image sequence with each one of the three temporal filters obtained (*low-pass* and two *band-pass* filters.)

Algorithm 1 outlines the basic behavior of the temporal filtering stage. Usually, for all stages, the calculation of the corresponding filter is performed off-line if

necessary, prior to computation. As the number of temporal filters usually remains constant and is reduced (i.e., $nTemp_filters = 3$), performance rates of this stage greatly depend on the window size (L) in which we apply the temporal filters and on frame dimensions ($nx \times ny$).

Algorithm 1 temp_filt = stage I (frames, N , L , $nTemp_filters$, α , τ)

```

for tf = 0 to  $nTemp\_filters$  do
  T_filters(tf) = get_temporal_filter( $\alpha$ ,  $\tau$ ) {Get filters}
  for fr = 0 to  $N - L$  do
    frame = framesin(fr)
    for all  $p = pixel \in frame$  do
      temp_filt[tf][ $p$ ]  $\leftarrow [p * T\_filters]$  {Convolve  $p \otimes$ 
      T_filters}
    end for
  end for
end for

```

As output, $nTemp_filters$ matrices of the same dimensions as each input frame are generated as a result of the convolution of each frame with the corresponding convolution filter. These matrices will be the input for the second stage (*spatial filtering*).

DSP optimizations and performance results Figure 4 reports the experimental results obtained after the implementation and optimization of the temporal filtering

stage. Throughput results are given in terms of frames per second, considering increasing square frame dimensions and increasing window sizes (L) for the temporal convolution. We do not report results for a different number of temporal filters, as three is the most common configuration for McGM. We compare the throughput attained by the basic implementation using one core, with that of a version with all the exposed optimizations applied on one core, and parallelized across the eight available cores in the C6678.

At this stage, the critical factors affecting performance are frame size ($nx \times ny$) and temporal window size (L). In general, for a fixed L , throughput decreases for increasing frame dimensions. For a fixed frame dimension, the impact of increasing the window size is also translated into a decrease in performance, although not in a relevant factor.

Independently from the evaluated frame resolution and window dimensions, core-level optimizations (usage of DMA, loop optimizations, and SIMD vectorization) are translated into performance improvements between $\times 1.5$ and $\times 2$, depending on the specific selected parameters. When OpenMP parallelization is applied, the throughput improvement yields between $\times 5.5$ and $\times 7$ compared with the optimized sequential version. In general, the throughput obtained by applying the complete set of optimizations improves the original basic implementation in a factor between $\times 7$ and $\times 14$. We would like to remark the multiplicative effects observed

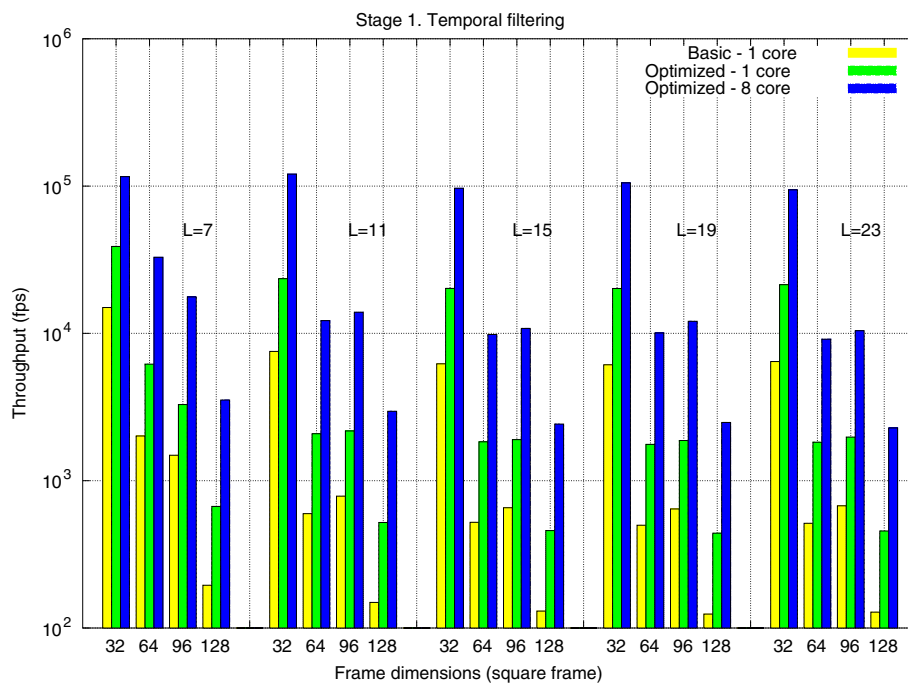


Figure 4 Throughput of the DSP implementation of the temporal filtering stage. For different frame dimensions and temporal window sizes.

when both in-core and multi-core optimizations are carried out.

4.2.2 Stage 2: spatial filtering

Algorithm and implementation From the algorithmic point of view, spatial filtering does not dramatically differ from the previous stage, see Algorithm 2. For each one of the spatial filters generated *a priori* and each one of the temporal-filtered frames, we apply a bi-dimensional convolution. Note that the amount of generated data increases compared with that received from the previous stage in a factor of $n_{\text{Spat_filters}}$. The window size in the convolution (T parameter) is the key in terms of precision and performance. As a result of this stage, we obtain a set of intermediate spatially filtered frames that will be provided as an input to the *steering* stage.

Algorithm 2 $\text{spat_filt} = \text{stage II}(\text{temp_filt}, N, L, n_{\text{Temp_filters}}, n_{\text{Spat_filters}}, T)$

```

for  $\text{sf} = 0$  to  $n_{\text{Spat\_filters}}$  do
     $\text{S\_filt}[\text{sf}] = \text{get\_spatial\_filter}(\text{sf})$  {Get filters}
end for
for  $\text{tf} = 0$  to  $n_{\text{Temp\_filters}}$  do
    for  $\text{fr} = 0 \leq N - L$  do
         $\text{frame} = \text{frames}_{\text{in}}(\text{fr})$ 
        for all  $p = \text{pixel} \in \text{frame}$  do
            for  $\text{sf} = 0$  to  $n_{\text{Spat\_filters}}$  do
                 $\text{spat\_filt}[\text{sf}][\text{tf}][p] \leftarrow \text{conv2D}(\text{temp\_filt}[\text{tf}][p], \text{S\_filters}(\text{sf}), T)$ 
            end for
        end for
    end for
end for

```

DSP optimizations and performance results Besides the basic implementation derived from the algorithmic definition of the stage, our optimizations (*loop optimization*, *vectorization*, and *parallelization*) are focused on the bi-dimensional convolution kernel in order to adapt it to DSP architecture specifications. More specifically, we leverage the separability of the bi-dimensional convolution to perform and highly optimize one-dimensional (1D) vertical and horizontal convolutions, applying optimizations at instruction level (loop unrolling), data level (vectorization in the 1D convolution loop body), and thread level across cores (through OpenMP).

Figure 5 reports the experimental results obtained after the implementation and optimization of the spatial filtering stage. Results are presented for different frame dimensions and increasing spatial window sizes. As previous considerations for the temporal stage, a comparison between a baseline version, an in-core-level optimization,

and optimized version across multi-core has also been performed.

At this stage, frame size ($n_x \times n_y$) and spatial window size (T) substantially impact performance rates. As for the previous stage, when fixing T , throughput decreases for increasing frame dimensions. However, for a fixed frame dimension, the impact of increasing the spatial window size is translated into higher throughput; from our analysis, our separate bi-dimensional convolution implementations attain better performance as window size increases, mainly due to the avoidance of memory latency effects. This improvement, though, is expected to stabilize for larger window sizes (that are usually not common in McGM).

Core-level optimizations are translated into performance improvements between $\times 1.6$ and $\times 2.2$, depending on the evaluated frame and window dimensions. The thread-level parallelization yields an improvement between $\times 5$ and $\times 6.5$ when comparing with the optimized sequential version. In general, the throughput obtained by applying the complete set of core-level optimizations and thread-level parallelization improves the original basic implementation in a factor between $\times 8$ and $\times 13$.

4.2.3 Stage 3: steering filtering

Algorithm and implementation Algorithm 3 describes the necessary steps to perform the *steering* stage in the McGM method. Basically, the algorithm proceeds by applying a convolution between each spatial-filtered frame obtained from the previous stage (I in the algorithm), and an oriented filter F^θ previously calculated. The response of each one of the temporal- and spatial-filtered frames to this oriented filter will be the output of this stage.

Algorithm 3 $R = \text{stage III}(\text{spac_filt}, N, L, n_{\text{Temp_filters}}, n_{\text{Spat_filters}}, n_{\text{Ortho_Orders}}, n_{\theta s})$

```

for  $\theta = 0$  to  $n_{\theta s}$  do
    for  $\text{oo} = 0$  to  $n_{\text{Ortho\_Orders}}$  do
        for  $\text{sf} = 0$  to  $n_{\text{Spat\_filters}}$  do
            for  $\text{tf} = 0$  to  $n_{\text{Temp\_filters}}$  do
                for  $\text{fr} = 0 \leq N - L$  do
                     $\text{frame} = \text{frames}_{\text{in}}(\text{fr})$ 
                    for all  $p = \text{pixel} \in \text{frame}$  do
                         $I = \text{spat\_filt}[\text{sf}][\text{tf}][p]$ 
                         $R^\theta[\text{oo}][\text{sf}][\text{tf}][p] \leftarrow [F^\theta * I]$  {Convolve  $F \otimes I$ }
                    end for
                end for
            end for
        end for
    end for

```

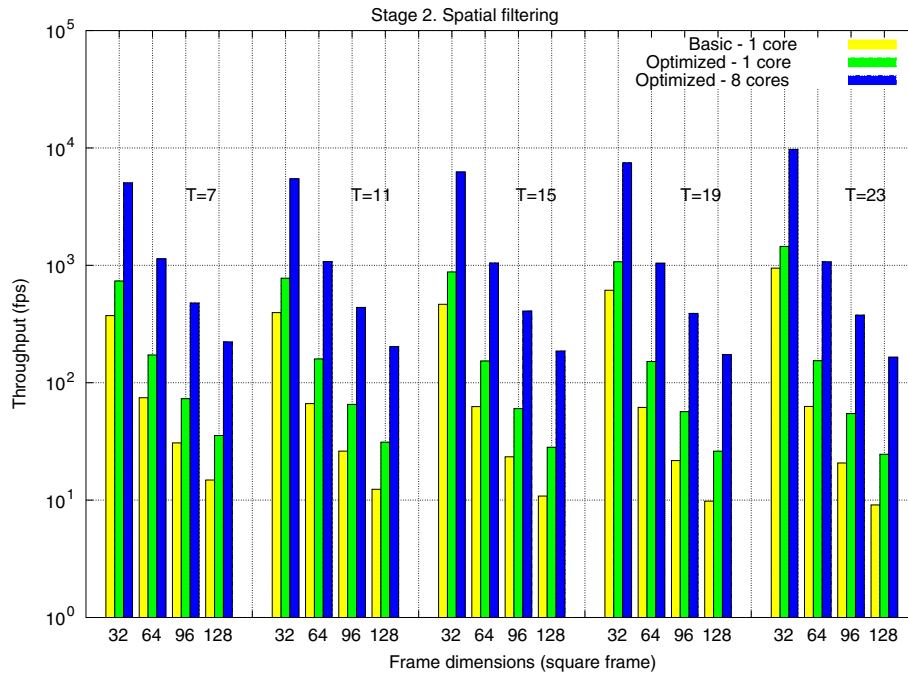


Figure 5 Throughput of the DSP implementation of the spatial filtering stage. For different frame dimensions and spatial window sizes.

DSP optimizations and performance results The optimizations applied to this stage are in the same way as those presented from the previous stages. Data parallelism is heavily exploited when possible, and loops are optimized after a deep search of the optimal unrolling parameters. OpenMP is used to extract thread-level parallelism and leverage the power of the eight cores in the C6678.

Special caution must be taken at this stage with memory consumption, as it reaches the maximum memory requirements of the McGM algorithm. More specifically, at this point, both the spatial-filtered frames and their steering filtering must coexist in the memory. However, this potential issue is conditioned by input algorithm parameters which are known beforehand.

Figure 6 reports the experimental results obtained after the implementation and optimization of the steering stage. Results are presented for different frame dimensions and different number of angles (orientations). As in previous stages, we compare the throughput attained by the basic implementation with that of a version with all the exposed core-level optimizations applied on one core, and with these optimizations together when the computation is distributed across eight cores.

At this stage, the factors affecting performance are frame size ($n_x \times n_y$) and number of orientations (n_θ s). For a fixed number of angles, throughput decreases for increasing frame dimensions. For a common resolution, increasing the number of angles considered also yields

higher throughput. Core-level optimizations are more significant here, being the reason the higher arithmetic intensity in the loop bodies. These optimizations yield performance improvements between $\times 4$ and $\times 5$, depending on the evaluated frame dimensions and number of angles. The thread-level parallelization yields an improvement between $\times 1.5$ and $\times 2.5$ taking as a reference the optimized sequential version, with higher improvements as the number of orientations is increased. In general, the throughput obtained by applying the complete set of optimizations outperforms the basic implementation in a factor between $\times 10$ and $\times 12.5$.

4.2.4 Final stages

Final stages are not considered in detail as they are mainly compressive from the data perspective and usually require a non-significant fraction of time. Related to this, Figure 7 reports a detailed analysis of the percentage of time devoted to each stage in a typical execution of the McGM algorithm. Similar results have been observed for other experimental configurations. In general, the first three stages of McGM consume around 90% of the total execution time. The remaining time is dedicated to compressive stages, memory management routines, and precalculation of filters previous to the execution. However, we observed similar benefits than those for the previous stages when applying the equivalent core-level and thread-level optimizations on the final stages, and they will be included in the global throughput results in Section 4.3.

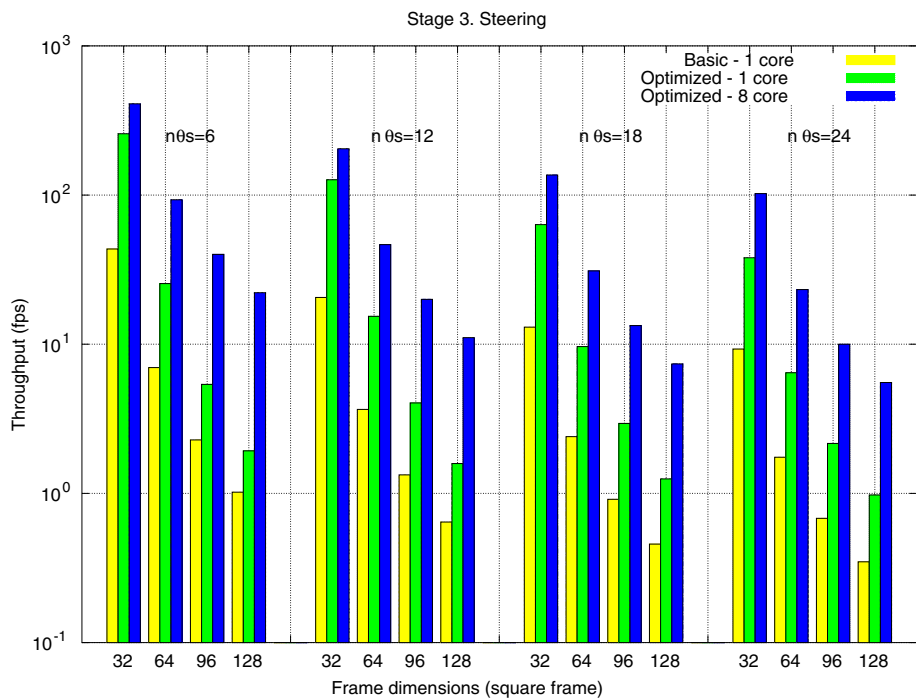


Figure 6 Throughput of the DSP implementation of the steering stage. For different frame dimensions and number of angles.

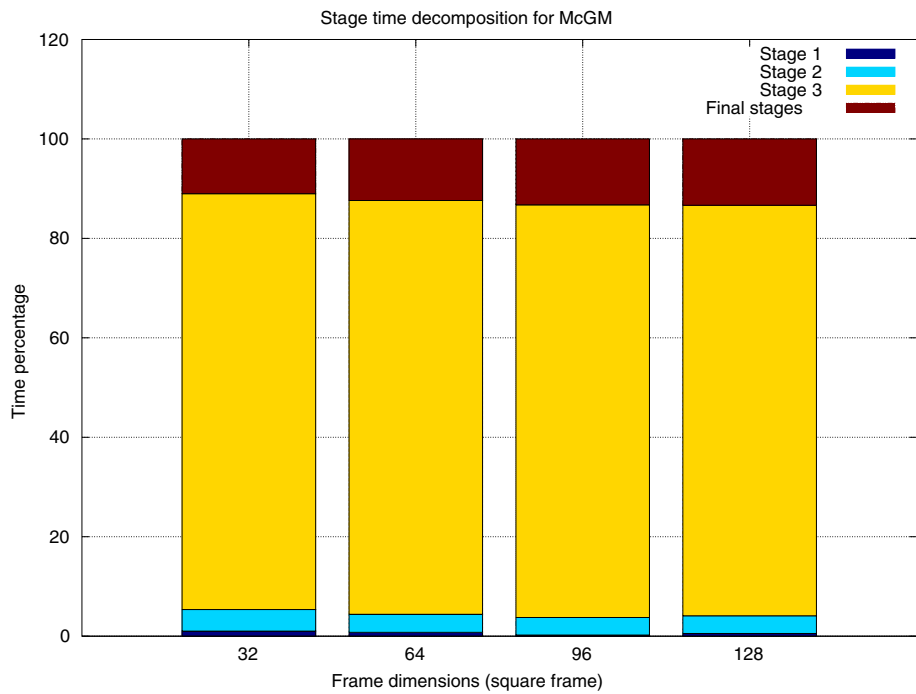


Figure 7 Time breakdown of the overall McGM implementation divided by stages.

Table 2 Throughput of the DSP implementation of McGM for different parameter configurations

	Throughput (fps)			
	32 ²	64 ²	96 ²	128 ²
Conf. 1	266.86	60.34	25.78	14.18
Conf. 2	343.15	54.83	21.39	11.27
Conf. 3	503.27	54.99	11.77	9.89
Conf. 4	650.71	57.48	19.45	9.79

4.3 Global throughput results and real-time considerations

Besides the isolated throughput attained by each individual stage of the algorithm analyzed in detail in previous sections, an overall view of the performance attained by the complete pipeline execution is necessary. Table 2 reports the throughput, in terms of frames per second, of the complete McGM implementation, considering only the most optimized version of each stage. Due to the wide variety of parameter combinations in the algorithm, we have chosen four different representative configurations, labeled as 'Conf. 1 to Conf. 4,' whose parameters are detailed in Table 1. Results are provided for increasing frame resolutions.

In general, throughput is reduced for increasing frame resolutions. While this rate is high for the minimum tested resolution (up to 650 fps for 32 × 32 frames), it dramatically decreases for larger frames, achieving a minimum of 9.74 fps for the largest resolution tested (128 × 128). Differences between several parameter configurations are specially significant for small frame dimensions but not critical for the rest. Comparing the global performance results with those for each one of the stages presented in Figures 4, 5, and 6, the main insight is that the *steering* stage is the clear limiting factor. Global throughput is far from that attained in the *temporal* and *spatial* filtering stages (that were in the order of thousands of frames per second, depending on the resolution) and

closer to that attained for the *steering* stage. This confirms the time breakdown detailed in Figure 7, which illustrates that 90% of the overall execution time is devoted to this stage.

In order to put results into perspective, Table 3 compares the throughput (in terms of frames per second) for a collection of platforms representative of current multi-core technology. We have selected a high-end general-purpose processor (Intel Xeon) and two different architectures as representatives of current low-power solutions, namely:

- TI DSP C6678 processor (eight cores) at 1 GHz with 512 Mbytes of RAM.
- Two Intel Xeon X5570 (eight cores in two sockets) at 2.93 GHz with 24 Gbytes of RAM.
- Intel Atom D510 (two cores) at 1.66 GHz with 2 Gbytes of RAM.
- ARM Cortex A9 (two cores) at 1 GHz (built by TI) with 1 Gbyte of RAM.

The table also reports the TDP in order to give an overview of the peak power consumption for each one of the platforms. Note that the TI C6678 DSP can be considered as a low-power architecture, especially compared with the Intel Xeon (10 vs. 190 W when the two sockets of the latter are used). However, it is still far from the reduced power dissipated by the ARM Cortex A9.

Clearly, the multi-threaded implementation of McGM on the eight cores of the Intel Xeon yields the highest throughput rate from all the evaluated frame dimensions. For input images of 128 × 128 pixels, the throughput rate is roughly 21 fps. When only one core of the Intel Xeon is used, this rate is reduced to 4 fps. Our optimized implementation on the C6678 DSP outperforms the sequential results on the Intel Xeon, achieving a peak rate for the largest tested frame dimensions of 9.74 fps. Considering a rate around 20 fps, acceptable for being considered as real-time processing (performance rates meeting real-time processing are in italic in Table 3), the parallel

Table 3 Throughput and power efficiency of McGM implementations on different architectures, using Conf. 4 and different frame sizes

Processor	TDP	Throughput (fps)				Power efficiency (kpps/watt)			
		32 ²	64 ²	96 ²	128 ²	32 ²	64 ²	96 ²	128 ²
Xeon (8c)	190 W	1,390.09	136.06	45.04	20.91	7.49	2.93	2.18	1.80
Xeon (1c)	95 W	1,065.41	34.55	9.70	3.99	11.48	1.49	0.94	0.68
C6678	10 W	650.71	57.48	19.45	9.79	66.63	23.54 ^a	17.93 ^a	15.95 ^a
Atom	13 W	182.76	5.62	3.02	1.23	14.39	1.77	2.14	1.55
Cortex A9	1.2 W	126.87	6.44	1.79	0.75	108.26 ^a	21.98	13.76	10.30

Numbers in italic meet real-time requirements. ^aThe best efficiency achieved for each frame size. kpps, thousands of pixels processed per second.

implementation on the Intel Xeon can attain real-time on resolutions up to 128×128 , meanwhile the TI DSP can attain real-time processing on up to 96×96 frame dimensions. Given the scalability observations extracted from our experimental results, we do not observe any relevant limitation for better performance results in future multi-core DSP architectures, possibly equipped with a larger number of cores.

4.4 Power efficiency considerations

This throughput rates must be considered in the context of the real power dissipated by each platform. To illustrate the power efficiency of each platform when executing McGM, Table 3 also provides a comparative analysis of the efficiency of each architecture in terms of thousands of pixels processed per second (kpps) per watt. The best power efficiency ratios are indicated with superscript letters in the table. Note that even though the ultra-low-power ARM is the most efficient architecture for the smallest input images (32×32), the TI DSP is clearly the most efficient platform for larger images. In this sense, the TI DSP offers a trade-off between performance and power that can be of wide appeal for those applications and scenarios in which power consumption is a restriction, but real time is still a requirement for medium/large image inputs.

General-purpose multi-core architectures deliver lower rates in terms of power efficiency but are a requirement if real-time processing is needed for the largest tested images. Compared with the other two low-power architectures (Intel Atom and ARM Cortex A9), real-time processing is only achieved for low-resolution images (32×32 in both cases). Thus, our DSP implementation, and the DSP architecture itself, can be considered as an appealing architecture not only when low power is desired but also when throughput is a limiting requirement.

5 Conclusions

In this paper, we have presented a detailed performance study of an optimized implementation of a robust motion estimation algorithm based of a gradient model (McGM) on a low-power multi-core DSP. Our study reports a general description of each stage of the multi-channel algorithm, with several optimizations that offer appealing throughput gains for a wide range of execution parameters.

We do not propose the TI DSP architecture as a replacement of high-end current architectures, like novel multi-core CPUs or many-core GPUs, but as an attractive solution for scenarios with tight power-consumption requirements. DSPs allow trade-off between performance, precision, and power consumption, with clear gains compared with other low-power architectures in terms of throughput (fps). In particular, while real-time

processing is attained only for low-resolution image sequences on current low-power architectures (typically 32×32 frames), our implementations elevates this condition up to images with resolution 96×96 or higher, depending on the inputs execution parameters. These results outperform those on a single core of a general-purpose processor and are highly competitive with optimized parallel versions in exchange of a dramatic reduction in power requirements.

These encouraging results open the chance to consider these architectures in mobile devices where power consumption is a severe limiting factor, but throughput is a requirement. Our power consumption considerations are based on estimated peak dissipated power as provided by manufactures in the processor specifications. Nevertheless, to be more accurate in terms of power consumption, we will consider as future work a more detailed energy evaluation study, offering real measurements at both core and system level.

Competing interests

The authors declare that they have no competing interests.

Acknowledgements

This work has been supported by Spanish Projects CICYT-TIN 2008/508 and TIN2012-32180.

Received: 31 January 2013 Accepted: 10 April 2013

Published: 10 May 2013

References

1. CL Huang, YT Chen, Motion estimation method using a 3D steerable filter. *Image Vision Comput.* **13**(1), 21–32 (1995)
2. BD Lucas, T Kanade, in *Proc. of 7th Int. Joint Conf. on Artificial Intelligence (IJCAI '81)*. An iterative image registration technique with an application to stereo vision (Morgan Kaufmann Publishers Inc, San Francisco, CA, USA, April 1981), pp. 674–679
3. H-S Oh, H-K Lee, Block-matching algorithm based on an adaptive reduction of the search area for motion estimation. *Real-Time Imaging.* **6**, 407–414 (October 2000)
4. D Sun, JP Lewis, Michaelj, in *Proc. ECCV*. Black. Learning optical flow (Brown University, Providence, Rhode Island 02912, USA, 2008), pp. 83–97
5. S Baker, R Gross, I Matthews, Lucas-kanade 20 years on: a unifying framework: part 3. *Int J Comput Vis.* **56**, 221–255 (2002)
6. X Liang, PW McOwan, A Johnston, Biologically inspired framework for spatial and spectral velocity estimations. *J. Opt. Soc. Am. A.* **28**(4), 713–723 (April 2011)
7. CP Benton, PW McOwan, A Johnston, Robust velocity computation from a biologically motivated model of motion perception. *Proc R Soc B.* **266**, 509–518 (1999)
8. A Johnston, CW Clifford, A unified account of three apparent motion illusions. *Vision Res.* **35**(8), 1109–1123 (April 1995)
9. F Ayuso, G Botella, C Garcia, M Prieto, F Tirado, GPU-based acceleration of bio-inspired motion estimation model. *Concurrency and Computation: Practice and Experience*, In press
10. GB Juan, Ríos García A, M Rodríguez-Alvarez, ER Vidal, U Meyer-Bäse, MC Molina, Robust bioinspired architecture for optical-flow computation. *IEEE Trans. VLSI Syst.* **18**(4), 616–629 (2010)
11. C Dhoot, VJ Mooney, SR Chowdhury, LP Chau, in *VLSI-SoC*. Fault tolerant design for low power hierarchical search motion estimation algorithms (IEEE Computer Society, Los Alamitos, CA (USA), 2011), pp. 266–271
12. Vleeschouwer De C, T Nilsson, in *ICIP (2)*. Motion estimation for low power video devices (IEEE Computer Society, Los Alamitos, CA (USA), 2001), pp. 953–956

13. M Anguita, J Díaz, E Ros, FJ Fernandez-Baldomero, Optimization strategies for high-performance computing of optical-flow in general-purpose processors. *IEEE Trans. Circuits Syst. Video Techn.* **19**(10), 1475–1488 (2009)
14. D Honegger, P Greisen, L Meier, P Tanskanen, M Pollefeys. *IROS* (IEEE, 2012), pp. 5177–5182
15. B Subramaniam, Wu-chun Feng, in *8th IEEE Workshop on High-Performance, Power-Aware Computing (HPPAC)*. The Green Index: A Metric for Evaluating System-Wide Energy Efficiency in HPC Systems (IEEE Computer Society, Los Alamitos, CA (USA), May 2012)
16. Y Shirai, J Miura, Y Mae, M Shiohara, H Egawa, S Sasaki, in *Computer Architectures for Machine Perception, 1993. Proceedings*. Moving object perception and tracking by use of dsp (IEEE Computer Society, Los Alamitos, CA (USA), Dec 1993), pp. 251–256
17. BKP Horn, BG Schunck, Determining optical flow. *Artif. Intell.* **17**, 185–203 (1981)
18. T Rvekamp, M Platzner, L Peters, in *In Proceedings of the 8th ICSPAT*. Specialized architectures for optical flow computation: A performance comparison of asic, dsp, and multi-dsp, (1997), pp. 829–833
19. A Steimer, in *Master Thesis. ETH Zurich*. Global optical flow estimation by linear interpolation algorithm on a DSP microcontroller, (Switzerland, October, 2011)
20. MV Srinivasan, An image-interpolation technique for the computation of optic flow and egomotion. *Biol. Cybernetics*. **71**, 401–415 (1994)
21. RJ Snowden, RF Hess, Temporal frequency filters in the human peripheral visual field. *Vision Res.* **32**(1), 61–72 (1992)
22. JJ Koenderink, Optic flow. *Vision Res.* **26**, 161–180 (1996)
23. TMS320C6678 Multicore Fixed and Floating-Point Digital Signal Processor. <http://www.ti.com/lit/ds/sprs691c/sprs691c.pdf>, February 2012. Texas Instruments Literature Number: SPRS691C
24. F Ayuso, G Botella, C Garcia, M Prieto, F Tirado, in *WPABA 2011*. GPU-based acceleration of bioinspired motion estimation model (IEEE Computer Society Washington, DC, USA, 2011)
25. F Ayuso, G Botella, C Garcia, M Prieto, F Tirado, in *21st Int. Conf. on Field Programmable Logic and Applications, Workshop on Computer Vision on Low-Power Reconfigurable Architectures, 2011*. GPU-based signal processing scheme for bioinspired optical flow (IEEE Computer Society, Los Alamitos, CA (USA), p. 2011. 09/2011 (2011)
26. Introduction to TMS320C6000 DSP optimization. <http://www.ti.com/lit/an/sprabf2/sprabf2.pdf>, October 2011. Texas Instruments Literature Number: SPRABF2

doi:10.1186/1687-6180-2013-99

Cite this article as: Igual et al.: Robust motion estimation on a low-power multi-core DSP. *EURASIP Journal on Advances in Signal Processing* 2013 **2013**:99.

Submit your manuscript to a SpringerOpen[®] journal and benefit from:

- Convenient online submission
- Rigorous peer review
- Immediate publication on acceptance
- Open access: articles freely available online
- High visibility within the field
- Retaining the copyright to your article

Submit your next manuscript at ► springeropen.com